

X-ray softening during the 2008 outburst of XTE J1810-189

Shan-Shan Weng^{1,2,3*} †, Shuang-Nan Zhang^{2,4,‡}, Shu-Xu Yi², Yu Rong², Xu-Dong Gao^{5,4}

¹ *Sabancı University, Faculty of Engineering and Natural Sciences, Orhanlı–Tuzla, İstanbul 34956, Turkey*

² *Key Laboratory of Particle Astrophysics, Institute of High Energy Physics, Chinese Academy of Sciences, Beijing 100049, China*

³ *Department of Physics, Xiangtan University, Xiangtan 411105, China*

⁴ *National Astronomical Observatories, Chinese Academy of Sciences, Beijing, 100012, China*

⁵ *Department of Astronomy, Beijing Normal University, Beijing 100875, China*

ABSTRACT

XTE J1810-189 underwent an outburst in 2008, and was observed over ~ 100 d by *RXTE*. Performing a time-resolved spectral analysis on the photospheric radius expansion burst detected on 2008 May 4, we obtain the source distance in the range of 3.5–8.7 kpc for the first time. During its outburst, XTE J1810-189 did not enter into the high/soft state, and both the soft and hard colours decreased with decreasing flux. The fractional rms remained at high values (~ 30 per cent). The *RXTE*/PCA spectra for 3–25 keV can be described by an absorbed power-law component with an additional Gaussian component, and the derived photon index Γ increased from 1.84 ± 0.01 to 2.25 ± 0.04 when the unabsorbed X-ray luminosity in 3–25 keV dropped from 4×10^{36} ergs s^{−1} to 6×10^{35} ergs s^{−1}. The relatively high flux, dense observations and broadband spectra allow us to provide strong evidence that the softening behaviour detected in the outburst of XTE J1810-189 originates from the evolution of non-thermal component rather than the thermal component (i.e. neutron star surface emission).

Key words: accretion, accretion discs — stars: distances — stars: neutron — X-rays: bursts — X-rays: individual (XTE J1810-189)

1 INTRODUCTION

X-ray binaries dominate the X-ray emission of our Galaxy, and hundreds of them have been detected in the Galaxy and the Magellanic Clouds (Liu et al. 2006, 2007). A low-mass X-ray binary (XRB) is a system in which a low-mass companion ($M < M_{\odot}$) feeds a black-hole (BH) or a weakly magnetized neutron star (NS) via Roche-lobe overflow. NS XRBs can be further classified into low luminosity atoll sources ($\sim 0.001 - 0.5 L_{\text{Edd}}$) and high luminosity Z sources ($L_X \sim L_{\text{Edd}}$) according to their X-ray spectra and timing properties (Hasinger & van der Klis 1989; van der Klis 2006). Because BHs and NSs have similar gravitational fields, it is difficult to distinguish BH XRBs and NS XRBs unless type I X-ray bursts or coherent pulsations are detected.

Type I X-ray bursts are sudden energy release processes caused by unstable thermonuclear burning on the surface of NSs in XRBs (e.g. Lewin, van Paradijs & Taam 1993). The burst spectrum can be described well by a blackbody (BB) component. In the special class burst events, the so-called photospheric radius expansion (PRE) bursts, the peak X-ray luminosity reaches and remains at the local Eddington luminosity for a few seconds, during which

the atmosphere is lifted up owing to strong radiation and the effective temperature decreases. At the moment of touchdown, the photosphere settles on the NS surface again, i.e. the radius derived from the BB normalization reaches a local minimum corresponding to the radius of a NS. Since the mass and surface red shift of NSs only vary in the narrow ranges, the Eddington luminosities measured from PRE bursts are good distance indicators (Basinska et al. 1984; Kuulkers et al. 2003).

The colour-colour diagram (CCD), in which both soft and hard colours are defined as the ratio of count rates between different energy bands, is particularly useful for characterizing the behaviour of NS XRBs (e.g., Munro, Remillard & Chakrabarty 2002). The complete CCD from atoll sources has a Z shape, consisting of, from top to bottom, the extreme island state, the island state, and the banana state (e.g., Gierliński & Done 2002). It has been suggested that, as accretion rates increase, atoll sources go through from the extreme island state to the banana state (e.g., Hasinger & van der Klis 1989). Following Lin, Remillard & Homan (2007), we describe the extreme island, island, banana states as low/hard, intermediate, and high/soft states, which are consistent with BH XRBs. Some observational phenomena indicate that the accretion rate might not monotonously increase when a source moves along the Z pattern, especially in the branch for the intermediate state (Galloway et al. 2008). The fast time variability, which can be characterized by the root mean square (rms), is another key tool for diagnosing accretion states in XRBs (e.g., Muñoz-Darias, Motta & Belloni 2011; Heil,

* E-mail: wengss@ihep.ac.cn

† Current address: Department of Physics and Institute of Theoretical Physics, Nanjing Normal University, Nanjing 210023, China

‡ E-mail: zhangsn@ihep.ac.cn

Vaughan & Uttley 2012). The positive correlation between rms and hardness (or colour) is commonly observed in outbursts of both BH and NS XRBs (Lin et al. 2007; Muñoz-Darias et al. 2014). That is, XRBs have low variability when their radiation is dominated by thermal emission and vice versa (Belloni 2010). However, this correlation is not well explored below $\sim 0.01L_{\text{Edd}}$.

As already stated above, stellar-mass BHs and NSs have similar compactness; therefore, BH XRBs and NS XRBs share many spectral and temporal properties at high luminosity ($L_X > 0.01L_{\text{Edd}}$; e.g., Done et al. 2007; Weng & Zhang 2011). Recently, much effort has been devoted to the differences between two classes of XRB at low luminosity ($L_X < 0.01L_{\text{Edd}}$): (1) Compared to BH XRBs, NS XRBs are less radio loud at a given X-ray luminosity, or in the other words, BH XRBs have a lower X-ray radiative efficiency resulting from the advection-dominated accretion flows (Migliari & Fender 2006); (2) For the comparable accretion, NS XRBs are brighter than BH XRBs by a factor of $\sim 100 - 1000$, owing to additional emission from their solid surface (Narayan & McClintock 2008); (3) As the luminosity decreases, it has been proposed (Weng & Zhang 2011) that accretion discs in NS XRBs begin to leave the innermost stable circular orbit at higher luminosity, i.e. the discs are truncated by the NS magnetospheres at low luminosity; (4) At $10^{34} - 10^{36} \text{ erg s}^{-1}$, NS XRBs have softer spectra, probably arising from the soft thermal component emitted by NSs surface, which contributes a significant fraction of X-ray emissions (Wijnands et al. 2014).

XTE J1810-189 underwent an outburst in 2008 and was monitored by *RXTE* from 2008 March 19 to 2008 June 19. Markwardt, Strohmayer & Swank (2008) detected a type I X-ray burst from the source, identifying it as a NS XRB, and also put an upper limit for distance of $\sim 11.5 \text{ kpc}$ according to the peak flux of the type I X-ray burst. To date, the *RXTE* data have not been systematically analyzed in the literature. In Section 2, we estimate the interstellar hydrogen column density (N_{H}) with *Swift*/XRT data, measure the distance according to the mean peak flux of PRE burst detected by *RXTE*, and also evaluate the spectral evolution of the 2008 outburst of XTE J1810-189. We discuss these results in Section 3, and the summary follows in Section 4.

2 DATA ANALYSIS & RESULTS

2.1 Estimate absorption column density using *Swift* data

Because *RXTE*/PCA is not sensitive to energies below 2 keV, the *Swift*/XRT spectra are analysed to constrain the absorption column density. Seven *Swift* pointing observations were made in 2008 March, and the other one was made on 2011 June 19. The initial event cleaning is performed with the task `xrtpipeline` with standard quality cuts. All XRT data were taken in photon-counting mode; however, all of them suffer from problems of pile-up because of high count rates $\sim 1.0\text{--}1.8 \text{ cts/s}$. We extract spectra within annular regions centered on the source position with the inner radius $\sim 6\text{--}8$ pixels. The exposures maps are generated with `xrtexpomap` to correct for bad columns, the ancillary response files are produced with the task `xrtmkarf`, and the response matrix files (v014) are taken from the CALDB database. To ensure valid results using χ^2 statistical analysis, the spectra are further grouped to have at least 30 counts per bin.

The *Swift*/XRT data in 2008 can be best fitted by an absorbed power-law model with the photon index in the range of 1.4–1.9; however, the poor statistics of the spectra do not permit

Obs.ID	Obs-Date	N_{H}	Γ/kT	$flux$	χ^2/dof
00031167001	2008-03-17	$3.81^{+0.49}_{-0.46}$	$1.6^{+0.3}_{-0.3}$	$4.0^{+0.7}_{-0.5}$	169.8/169
00306737000	2008-03-18	...	$1.7^{+0.3}_{-0.3}$	$4.9^{+0.8}_{-0.6}$...
00031167002	2008-03-21	...	$1.4^{+0.3}_{-0.3}$	$5.0^{+0.7}_{-0.5}$...
00031167003	2008-03-22	...	$1.4^{+0.2}_{-0.2}$	$5.6^{+0.7}_{-0.5}$...
00031167004	2008-03-23	...	$1.4^{+0.2}_{-0.2}$	$5.2^{+0.6}_{-0.5}$...
00031167005	2008-03-24	...	$1.4^{+0.2}_{-0.2}$	$6.6^{+0.8}_{-0.6}$...
00031167006	2008-03-25	...	$1.9^{+0.3}_{-0.3}$	$6.4^{+1.4}_{-1.0}$...
00455640000	2011-06-19	$3.58^{+0.58}_{-0.50}$	$0.83^{+0.06}_{-0.06}$	$2.7^{+0.4}_{-0.3}$	31.5/38

Table 1. *Swift*/XRT spectra taken in 2008 are fitted by an absorbed power-law model, and the spectrum in 2011 is fitted by an absorbed BB model (*phabs*bbbodyrad* in XSPEC). N_{H} : Absorption column density in units of 10^{22} cm^{-2} . $flux$: 0.5–10 keV unabsorbed flux in units of $10^{-10} \text{ erg cm}^{-2} \text{ s}^{-1}$. All errors are in 90% confidence level.

two-component modelling. We fit these spectra simultaneously and link the hydrogen column density to have a common value, yielding $N_{\text{H}} = 3.81^{+0.49}_{-0.46} \times 10^{22} \text{ cm}^{-2}$ (Table 1), consistent with the value reported by Starling, Kennea & Krimm (2008). The spectrum for 2011 June 19 is very soft with $\Gamma = 3.70^{+0.40}_{-0.36}$, indicating that the emissions are dominated by the thermal component. Compared with the power-law model ($\chi^2/dof = 41.1/38$), the absorbed blackbody (BB) model provides much better fits to the data ($\chi^2/dof = 31.5/38$), and the obtained $N_{\text{H}} = 3.58^{+0.58}_{-0.50} \times 10^{22} \text{ cm}^{-2}$ is consistent with the results derived from the data in 2008. Thus, we adopt $N_{\text{H}} = 3.81^{+0.49}_{-0.46} \times 10^{22} \text{ cm}^{-2}$ for the following *RXTE* spectral analysis.

2.2 Properties of persistent emission

All 59 *RXTE* data of XTE J1810-189 taken by the Proportional Counter Array (PCA) are analysed with the FTOOLS software package version 6.13. The persistent emission, i.e. the X-ray emission when the type I X-ray bursts are not present, is extracted from the Standard2 data from the top layer of PCU2 with the standard criteria: the Earth-limb elevation angle is larger than 10° and the spacecraft pointing offset is less than 0.02° . The background files are created using the program `pcabackest`, while the latest bright background model is adopted for the first 43 observations and the faint background model is used for the last 16 observations, because the source count rate is less than 40 counts s^{-1} per PCU. Nevertheless, we checked that our results are not sensitive to the background model. Type I X-ray bursts are recorded in four observations (Fig. 1), in which the data of 300 s before and 1000 s after the type I X-ray bursts are excluded. The background-subtracted light curves are created and their count rates are averaged for each observation. The CCD of XTE J1810-189 is plotted in Fig. 2. We define the soft colour as the ratio of the count rates in the PCA channels of 9–11 (3.6–5.0 keV) and 0–8 (2.2–3.6 keV), and define the hard colour as the ratio of the count rates in the PCA channels of 21–43 (8.6–18.0 keV) and 12–20 (5.0–8.6 keV), respectively. In the 2008 outburst, the source evolved from the top right corner to the lower left corner, and both soft and hard colours were tightly correlated with the intensity (in 2.2–18.0 keV, Fig. 3).

The light curves, in the same PCA channels (0–43) as those used for producing the CCD, are extracted from the PCA Event mode data, `E_125us_64M_0_1s` for timing analysis. The power density spectra (PDS) are constructed using light curve segments of 32 s and 8 ms time bins with the task `powspec` (version 1.0). We adopt the method of Miyamoto to normalize the PDSs (Miyamoto,

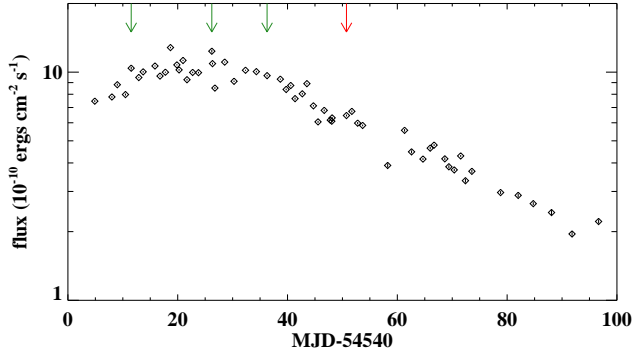


Figure 1. The light curve of XTE J1810-189 during its 2008 outburst. The unabsorbed flux in 3–25 keV is derived from the power-law fit (Table 2). The arrows label the observations in which the type I bursts are detected, and the last (red) one corresponds to the PRE burst.

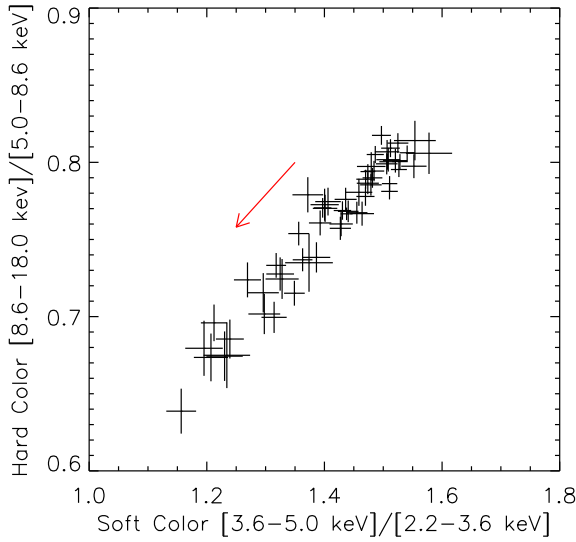


Figure 2. Colour-colour diagram of XTE J1810-189. The red arrow labels the direction of flux decay.

Kimura & Kitamoto 1991), and average them with the logarithmic rebinned option -1.03 for each observation. The Poisson noise is subtracted ($\text{norm} = -2$), and the fractional rms is integrated over the 0.1–10 Hz frequency band. As can be seen in Fig. 3, XTE J1810-189 displays a high and nearly constant variability level (~ 30 per cent rms) during the outburst.

The response matrix files are created by the generator PCARMF (v11.7), and the recommended systematic error of 0.5% is applied for the spectral analysis. The persistent emission is fitted for 3–25 keV by an absorbed power-law model with the N_H fixed to $3.81 \times 10^{22} \text{ cm}^{-2}$. An additional Gaussian component is required to mimic an iron line at ~ 6.4 keV. This model adequately fits all spectra with the reduced χ^2 values in the range 0.65 – 2.26. Only three observations with relatively long exposure time (observation IDs: 93044-7-03-00, 93433-01-05-04, and 93433-01-06-03) have the reduced χ^2 larger than 2. The worse fits might be due to strong

Obs.ID	MJD	Exp.(s)	Γ	Flux	χ^2/dof
93044-07-03-00	54544.9	6080	$1.94^{+0.02}_{-0.02}$	$7.46^{+0.07}_{-0.07}$	100.5/45
93044-07-04-00	54548.0	1968	$1.95^{+0.02}_{-0.02}$	$7.79^{+0.06}_{-0.06}$	68.9/45
93044-07-04-01	54549.0	992	$1.89^{+0.02}_{-0.02}$	$8.81^{+0.09}_{-0.09}$	53.1/45
93044-07-04-02	54550.5	1248	$1.90^{+0.02}_{-0.02}$	$7.98^{+0.08}_{-0.08}$	30.6/45
93044-07-05-00	54552.9	2624	$1.88^{+0.01}_{-0.01}$	$9.47^{+0.06}_{-0.06}$	48.2/45
93044-07-05-01	54551.5	448	$1.87^{+0.03}_{-0.03}$	$10.40^{+0.14}_{-0.14}$	41.3/45
93044-07-06-00	54553.7	1232	$1.87^{+0.02}_{-0.02}$	$10.03^{+0.09}_{-0.09}$	42.5/45
93433-01-01-00	54555.9	2608	$1.86^{+0.01}_{-0.01}$	$10.64^{+0.06}_{-0.06}$	62.8/45
93433-01-01-01	54556.8	3184	$1.92^{+0.01}_{-0.01}$	$9.62^{+0.06}_{-0.06}$	85.1/45
93433-01-01-02	54557.8	3200	$1.90^{+0.01}_{-0.01}$	$10.00^{+0.06}_{-0.06}$	66.2/45
93433-01-01-03	54558.7	1376	$1.84^{+0.01}_{-0.01}$	$12.81^{+0.09}_{-0.09}$	31.6/45
93433-01-01-04	54559.8	2912	$1.87^{+0.01}_{-0.01}$	$10.76^{+0.06}_{-0.06}$	62.2/45
93433-01-02-00	54560.3	1232	$1.89^{+0.02}_{-0.02}$	$10.23^{+0.09}_{-0.09}$	72.3/45
93433-01-02-01	54561.0	1920	$1.85^{+0.01}_{-0.01}$	$11.25^{+0.07}_{-0.07}$	54.4/45
93433-01-02-02	54561.7	1408	$1.89^{+0.02}_{-0.02}$	$9.27^{+0.08}_{-0.08}$	47.7/45
93433-01-02-03	54562.7	2064	$1.86^{+0.01}_{-0.01}$	$9.98^{+0.07}_{-0.07}$	55.3/45
93433-01-02-04	54563.8	1440	$1.88^{+0.02}_{-0.02}$	$9.95^{+0.08}_{-0.08}$	50.8/45
93433-01-02-05	54566.2	320	$1.84^{+0.03}_{-0.03}$	$12.35^{+0.18}_{-0.18}$	50.0/45
93433-01-02-06	54566.3	1136	$1.86^{+0.02}_{-0.02}$	$10.90^{+0.09}_{-0.09}$	52.3/45
93433-01-02-07	54566.8	1376	$1.95^{+0.02}_{-0.02}$	$8.52^{+0.08}_{-0.08}$	61.9/45
93433-01-03-00	54568.6	2720	$1.87^{+0.01}_{-0.01}$	$11.07^{+0.06}_{-0.06}$	73.7/45
93433-01-03-01	54570.3	1952	$1.91^{+0.01}_{-0.01}$	$9.12^{+0.07}_{-0.07}$	49.4/45
93433-01-03-02	54572.3	3312	$1.87^{+0.01}_{-0.01}$	$10.19^{+0.06}_{-0.06}$	69.5/45
93433-01-04-00	54574.3	1552	$1.88^{+0.01}_{-0.01}$	$10.05^{+0.08}_{-0.08}$	49.2/45
93433-01-04-01	54576.3	1552	$1.91^{+0.02}_{-0.02}$	$9.66^{+0.08}_{-0.08}$	47.5/45
93433-01-04-02	54578.7	2896	$1.91^{+0.01}_{-0.01}$	$9.32^{+0.06}_{-0.06}$	88.7/45
93433-01-04-03	54579.8	1728	$1.97^{+0.02}_{-0.02}$	$8.40^{+0.07}_{-0.07}$	74.3/45
93433-01-04-04	54580.6	2288	$1.92^{+0.01}_{-0.01}$	$8.74^{+0.06}_{-0.06}$	56.2/45
93433-01-05-00	54581.4	1248	$1.95^{+0.02}_{-0.02}$	$7.66^{+0.08}_{-0.08}$	47.1/45
93433-01-05-01	54582.7	1664	$1.95^{+0.02}_{-0.02}$	$8.04^{+0.07}_{-0.07}$	64.2/45
93433-01-05-02	54583.5	1952	$1.89^{+0.01}_{-0.01}$	$8.91^{+0.07}_{-0.07}$	60.9/45
93433-01-05-03	54584.7	3040	$1.94^{+0.01}_{-0.01}$	$7.12^{+0.05}_{-0.05}$	68.0/45
93433-01-05-04	54585.6	2208	$1.98^{+0.02}_{-0.02}$	$6.06^{+0.06}_{-0.06}$	101.5/45
93433-01-05-05	54586.7	1760	$1.96^{+0.02}_{-0.02}$	$6.80^{+0.06}_{-0.06}$	56.8/45
93433-01-05-06	54587.8	3200	$1.98^{+0.01}_{-0.01}$	$6.16^{+0.05}_{-0.05}$	77.0/45
93433-01-06-00	54588.1	1280	$1.98^{+0.02}_{-0.02}$	$6.10^{+0.07}_{-0.07}$	64.4/45
93433-01-06-01	54588.1	1680	$1.97^{+0.02}_{-0.02}$	$6.31^{+0.06}_{-0.06}$	58.5/45
93433-01-06-02	54590.7	1824	$1.99^{+0.02}_{-0.02}$	$6.46^{+0.06}_{-0.06}$	45.8/45
93433-01-06-03	54591.7	3200	$1.95^{+0.02}_{-0.02}$	$6.73^{+0.07}_{-0.07}$	100.5/45
93433-01-06-04	54592.8	1312	$2.00^{+0.02}_{-0.02}$	$5.98^{+0.07}_{-0.07}$	48.5/45
93433-01-06-05	54593.7	2416	$2.00^{+0.02}_{-0.02}$	$5.84^{+0.05}_{-0.05}$	74.6/45
93433-01-07-00	54598.2	656	$2.09^{+0.04}_{-0.04}$	$3.90^{+0.08}_{-0.08}$	49.8/45
93433-01-07-02	54601.3	1184	$1.96^{+0.02}_{-0.02}$	$5.56^{+0.07}_{-0.07}$	42.8/45
93433-01-08-00	54602.6	1104	$2.08^{+0.03}_{-0.03}$	$4.47^{+0.07}_{-0.07}$	34.3/45
93433-01-08-01	54604.7	3184	$2.10^{+0.02}_{-0.02}$	$4.16^{+0.04}_{-0.04}$	55.3/45
93433-01-08-02	54606.7	3168	$2.05^{+0.02}_{-0.02}$	$4.79^{+0.04}_{-0.04}$	62.3/45
93433-01-08-03	54608.7	1664	$2.07^{+0.03}_{-0.03}$	$4.17^{+0.06}_{-0.06}$	59.8/45
93433-01-08-04	54606.0	1536	$2.07^{+0.02}_{-0.02}$	$4.65^{+0.06}_{-0.06}$	47.3/45
93433-01-09-00	54609.4	1392	$2.11^{+0.03}_{-0.03}$	$3.85^{+0.06}_{-0.06}$	40.0/45
93433-01-09-01	54610.4	2224	$2.14^{+0.02}_{-0.02}$	$3.73^{+0.05}_{-0.05}$	47.3/45
93433-01-09-02	54611.5	3200	$2.08^{+0.02}_{-0.02}$	$4.29^{+0.04}_{-0.04}$	61.5/45
93433-01-09-03	54612.4	1008	$2.19^{+0.04}_{-0.04}$	$3.34^{+0.06}_{-0.06}$	35.9/45
93433-01-09-04	54613.6	1408	$2.13^{+0.03}_{-0.03}$	$3.68^{+0.06}_{-0.06}$	48.8/45
93433-01-10-00	54618.8	2288	$2.14^{+0.03}_{-0.03}$	$2.97^{+0.04}_{-0.04}$	51.2/45
93433-01-10-02	54622.0	1296	$2.18^{+0.04}_{-0.04}$	$2.88^{+0.05}_{-0.05}$	41.2/45
93433-01-11-00	54624.8	2400	$2.19^{+0.03}_{-0.03}$	$2.65^{+0.04}_{-0.04}$	49.9/45
93433-01-11-01	54628.1	960	$2.21^{+0.05}_{-0.05}$	$2.42^{+0.06}_{-0.06}$	29.3/45
93433-01-12-00	54631.8	2432	$2.25^{+0.04}_{-0.04}$	$1.95^{+0.04}_{-0.04}$	49.3/45
93433-01-12-01	54636.7	1488	$2.21^{+0.04}_{-0.04}$	$2.22^{+0.05}_{-0.05}$	45.2/45

Table 2. Spectra are fitted by an absorbed power-law model. Exp: Exposure time in units of second. Flux: 3–25 keV unabsorbed flux in units of $10^{-10} \text{ erg cm}^{-2} \text{ s}^{-1}$. All errors are for the 90% confidence level.

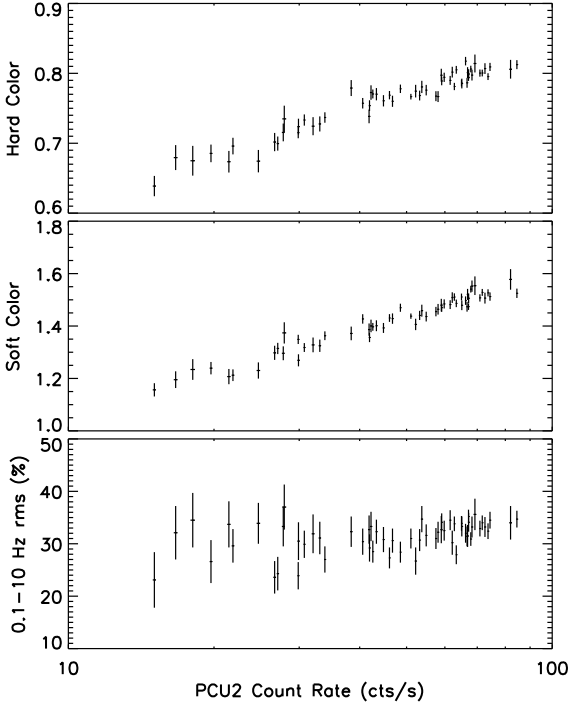


Figure 3. Panels from top to bottom show the hard colour, soft colour, and fractional rms plotted as the function of the PCU2 count rate (in 2.2–18.0 keV), respectively.

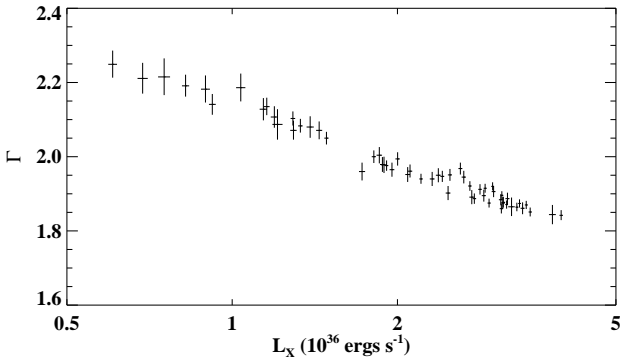


Figure 4. Spectra soften when the X-ray luminosity ($d = 5.1$ kpc is used) decrease.

spectral fluctuation; therefore, we assign a typical relative error of $\sim 1\%$ to Γ for these data (Table 2). The unabsorbed flux is calculated with the convolution model, *cflux*. As can be seen in Fig. 4, the spectra become softer when the X-ray flux decreases.

2.3 Evaluate source distance from PRE burst

The PCA Event mode data are analysed to study the PRE burst detected on 2008 May 4 (observation ID = 93433-01-06-02). We extract the time-resolved spectra of PRE burst within a time bin size

of 0.25 s around the burst peak, and use the longer integration time to compensate for the flux decay in the burst tail. Since the count rate of persistent emission is relatively low (~ 60 cts/s), we extract the spectrum from the whole observation in burst-free intervals to minimize the fluctuation, and the spectrum is used as the background for the PRE burst spectral modelling. The dead time effect is corrected following the approach suggested by the *RXTE* team¹. The spectra are fitted by a BB model (*phabs*bbbodyrad* in XSPEC), and the C statistic is used to accommodate low count rates. The fittings are generally performed over the energy range of 3–20 keV but concentrated to 3–18 keV or 3–15 keV to avoid unphysical parameters (mostly for the spectra at the late stage). For this observation, only PCU2 was on and channel 11 had zero counts; therefore, this channel is ignored in the fitting.

The derived parameters are plotted in Fig. 5, in which the red dashed lines mark the moment of touchdown. The bolometric flux of a burst is evaluated from the *bbbodyrad* model as:

$$F_{\text{bol}} = 1.076 \times 10^{-11} kT_{\text{BB}}^4 N_{\text{BB}} \text{ ergs cm}^{-2} \text{ s}^{-1}, \quad (1)$$

where kT_{BB} is the BB temperature in units of keV, and N_{BB} is the normalization. The measured flux is lower than the locally observed value by a factor of $(1 + z(R))^{-2}$ due to the gravitational red shift, where the red-shift factor $z(R) = \frac{1}{\sqrt{1 - \frac{2GM}{Rc^2}}} - 1$ (Lewin et al. 1993). Because the photosphere is lifted up to higher radius (smaller $z(R)$), the mean peak flux of PRE burst $F_{\text{peak,PRE}} = (5.09 \pm 0.30) \times 10^{-8} \text{ ergs cm}^{-2} \text{ s}^{-1}$ is slightly larger than the touchdown flux: $F_{\text{TD}} = (4.08 \pm 0.31) \times 10^{-8} \text{ ergs cm}^{-2} \text{ s}^{-1}$. Since there is only a small discrepancy between $F_{\text{peak,PRE}}$ and F_{TD} , we adopt the standard process, i.e. using $F_{\text{peak,PRE}}$ as the Eddington luminosity (from the NS surface) to minimize the fluctuation of spectral fitting.

We calculate the distance of XTE J1810-189 according to

$$d = 8.6 \left(\frac{F_{\text{peak,PRE}}}{3 \times 10^{-8} \text{ ergs cm}^{-2} \text{ s}^{-1}} \right)^{-1/2} \left(\frac{M_{\text{NS}}}{1.4 M_{\odot}} \right)^{1/2} \times \left[\frac{1 + z(R)}{1.31} \right]^{-1/2} (1 + X)^{-1/2} \text{ kpc}, \quad (2)$$

given by Galloway et al. (2008), where M_{NS} is the mass of NS and X is the hydrogen mass fraction in the atmosphere. Assuming the typical values $M_{\text{NS}} = 1.4 M_{\odot}$, $z(R) = 0.31$ (for $M_{\text{NS}} = 1.4 M_{\odot}$ and $R_{\text{NS}} = 10$ km), and $X = 0.7$ (cosmic abundances), we obtain $d = 5.1 \pm 0.2$ kpc, that is significantly smaller than the upper limit (~ 11.5 kpc) reported by Markwardt et al. (2008).

3 DISCUSSIONS

Fig. 3 shows that both the soft and hard colours decrease as the flux decays, and the fractional rms remains at ~ 30 per cent. Even though the values of both colours are consistent with an intermediate state, both the low luminosity and the strong variability point to a low/hard state for the atoll source. Accretion states of XRBs have been well explored at high luminosity, and colour variations are interpreted as the coevolution of both thermal and non-thermal components. Generally, compared to cases in the high/soft state, the accretion disc in the low/hard state is cooler, the power-law component becomes harder (smaller Γ), and the power-law fraction increases (e.g. Dunn et al. 2010; Muñoz-Darias et al. 2013). However, a study of the spectral evolution at low luminosity, when the

¹ http://heasarc.nasa.gov/docs/xte/recipes/pca_deadtime.html

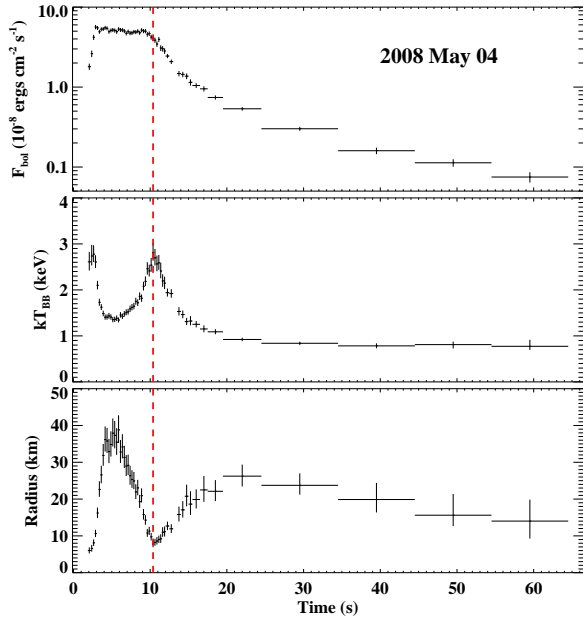


Figure 5. Time-resolved spectra of PRE burst are fitted by the absorbed BB model, and the radius of BB emission is derived by assuming $d = 10$ kpc. The red dashed lines mark the onset of touchdown.

contribution of accretion disc is negligible, is challenged by the low flux. Currently, collecting a sample of spectra at 0.5–10 keV for NS XRBs (i.e. taken from *Chandra/XMM-Newton/Swift*), Wijnands et al. (2014) suggested that the photon index increases with decreasing X-ray luminosity between 10^{34} and 10^{36} ergs s^{-1} , and BH XRBs have significantly harder spectra at the same luminosity (Armas Padilla et al. 2011; Plotkin, Gallo & Jonker 2013). However, because of the sparse data points for each source and large scatter on Γ , the anti-correlation between Γ and the X-ray luminosity is relatively weak. Moreover, it is difficult to reveal the nature of spectral softening with the limited band spectra (0.5–10 keV), and two possible scenarios have been proposed (see also Allen et al. 2015): (1) The thermal emission from the NS surface becomes the major component at the low luminosity. (2) The power-law component softens as the X-ray luminosity decrease to 10^{35} erg s^{-1} , below which the thermal component and another harder power-law component start to overcome the original power-law emission.

In this work, we reveal that the significant softening process occurs in the 2008 outburst of XTE J1810-189 in the flux range of $(2 - 13) \times 10^{-10}$ ergs $cm^{-2} s^{-1}$, which is well above the PCA background level. Since the PCA spectra in 3–25 keV provide a good constraint on the power-law component, the tight correlation between Γ and the X-ray luminosity with the dense *RXTE* observations is found in Fig. 4. Fitting all these data with the function $\Gamma = a \log L_X + b$ using the error of Γ as the weight, we obtain the coefficients: $a = -0.52 \pm 0.01$, $b = 20.8 \pm 0.5$. The source has $\Gamma \geq 2.1$ at $L_X \leq 10^{36}$ ergs s^{-1} , that is softer than spectra of most BH XRBs at the same luminosity.

To check whether the softening spectra result from a larger contribution of NS surface emissions, we refit the data using the model with an additional BB component included (*phabs*(powerlaw+bbbodyrad+gau)* in XSPEC). Because *RXTE*/PCA is not sensitive at the energy band below 3 keV, the

surface temperature kT is allowed to vary, but restricted to below 5 keV to avoid unphysical parameters (Table 3). As can be seen, the thermal component only contributes a small fraction ($< 10\%$) of the total flux and becomes cooler as the flux decays. Since the main part of BB component with $kT \leq 1$ keV is out of the coverage of PCA, its unabsorbed flux in 3–25 keV is less constrained. When the thermal component is added, the non-thermal component becomes slightly harder with a larger error in Γ . Nonetheless, the softening trend still emerges in the fitting; that is, Γ increases from $1.67^{+0.06}_{-0.07}$ to $2.10^{+0.09}_{-0.15}$. The high and constant variability levels indicate that the emissions in 3–25 keV are dominated by the non-thermal component, and the fractional contribution of the thermal component does not increase with decreasing flux. Note that the model’s independent parameter, the hard colour $((8.6-18.0)/(5.0-8.6)$ keV) also decreases following the flux decays (Fig. 3). Therefore, we demonstrate that the softer spectra at lower luminosity are caused by the softening of the power-law component.

The largest uncertainty in our results arises from the distance of the source, which depends on M_{NS} , $R_{NS}(z)$, and the composition of accretion material X . The caveats for using PRE bursts as the distance indicator are: (1) The Eddington luminosities vary from source to source (Kuulkers et al. 2003) and (2) even in the same source, PRE bursts could reach different peak fluxes due to the variation of burst fuel composition (Galloway et al. 2008). Assuming that M_{NS} , R_{NS} , and X are uniformly distributed in the typical range of $0.8 - 2.0 M_{\odot}$, $8 - 16$ km (e.g. Lattimer & Prakash. 2007; Steiner, Lattimer & Brown 2010), and 0 – 1, respectively, while $F_{\text{peak,PRE}} = (5.09 \pm 0.30) \times 10^{-8}$ ergs cm^{-2} having a normal distribution, we randomly generate 100 points for each parameters, then calculate 10^8 of d according to Equation (2). The simulated d has values in the range of 3.5 – 8.7 kpc, and the Gaussian fit to the profile of its distribution indicates $d = (5.5 \pm 1.7)$ kpc. Thus, we suggest that the L_X used above could vary by a factor of 3 at most, which would not change our conclusions.

4 SUMMARY

Investigating the X-ray archival data, we determined the distance of XTE J1810-189 as 3.5–8.7 kpc via the PRE burst for the first time. The source presents some peculiar X-ray behaviours, which distinguish it from most other NS XRBs: (1) During the 2008 outburst, XTE J1810-189 did not enter into the high/soft state, and moved steadily from the top right corner to the lower left corner in the CCD as the accretion rate decreased, as if the X-ray luminosity were proportional to the accretion rate; (2) The source is highly variable, and the fractional rms remains at a nearly constant level of ~ 30 per cent with evolving spectra; (3) Both soft and hard colours increase with the intensity. As the X-ray luminosity decreased from 4×10^{36} ergs s^{-1} to 6×10^{35} ergs s^{-1} , the X-ray spectra became softer with the photon index Γ increasing from 1.84 ± 0.01 to 2.25 ± 0.04 . The dense observations, relatively high flux and broadband spectra allow us to provide the strong evidence for softening of the non-thermal component (rather than NS surface emissions as suggested in literature) at low luminosity. Our results also confirm that NS XRBs have softer spectra below 10^{36} erg s^{-1} than those of BH XRBs, indicating there are different accretion mechanisms in two classes of XRBs, probably due to the boundary layer existing in NS XRBs.

Obs.ID	MJD	Γ	kT (keV)	f_{BB}	Flux	χ^2/dof
93044-07-03-00	54544.9	$1.77^{+0.04}_{-0.04}$	$1.01^{+0.06}_{-0.07}$	$0.56^{+0.14}_{-0.13}$	$7.63^{+0.04}_{-0.04}$	38.1/43
93044-07-04-00	54548.0	$1.75^{+0.06}_{-0.06}$	$0.94^{+0.08}_{-0.09}$	$0.60^{+0.19}_{-0.18}$	$7.99^{+0.07}_{-0.07}$	33.7/43
93044-07-04-01	54549.0	$1.79^{+0.08}_{-0.08}$	$1.00^{+0.19}_{-0.33}$	$0.40^{+0.32}_{-0.29}$	$8.95^{+0.10}_{-0.10}$	47.6/43
93044-07-04-02	54550.5	$1.77^{+0.08}_{-0.08}$	$1.14^{+0.13}_{-0.15}$	$0.51^{+0.30}_{-0.30}$	$8.09^{+0.09}_{-0.09}$	22.7/43
93044-07-05-00	54552.9	$1.76^{+0.05}_{-0.05}$	$1.02^{+0.13}_{-0.13}$	$0.50^{+0.21}_{-0.20}$	$9.56^{+0.06}_{-0.06}$	28.0/43
93044-07-05-01	54551.5	$1.70^{+0.10}_{-0.11}$	$1.06^{+0.15}_{-0.20}$	$0.72^{+0.47}_{-0.44}$	$10.60^{+0.16}_{-0.16}$	33.6/43
93044-07-06-00	54553.7	$1.74^{+0.07}_{-0.07}$	$1.11^{+0.11}_{-0.13}$	$0.63^{+0.31}_{-0.31}$	$10.18^{+0.09}_{-0.09}$	30.4/43
93433-01-01-00	54555.9	$1.72^{+0.05}_{-0.05}$	$1.10^{+0.07}_{-0.09}$	$0.70^{+0.24}_{-0.23}$	$10.82^{+0.07}_{-0.07}$	34.7/43
93433-01-01-01	54556.8	$1.75^{+0.04}_{-0.05}$	$1.07^{+0.06}_{-0.07}$	$0.73^{+0.20}_{-0.19}$	$9.78^{+0.06}_{-0.06}$	42.5/43
93433-01-01-02	54557.8	$1.77^{+0.04}_{-0.04}$	$1.02^{+0.09}_{-0.11}$	$0.54^{+0.20}_{-0.19}$	$10.16^{+0.06}_{-0.06}$	38.9/43
93433-01-01-03	54558.7	$1.75^{+0.06}_{-0.06}$	$1.18^{+0.14}_{-0.16}$	$0.58^{+0.35}_{-0.35}$	$12.96^{+0.10}_{-0.10}$	23.9/43
93433-01-01-04	54559.8	$1.74^{+0.04}_{-0.05}$	$1.12^{+0.08}_{-0.09}$	$0.67^{+0.23}_{-0.23}$	$10.92^{+0.07}_{-0.06}$	36.0/43
93433-01-02-00	54560.3	$1.67^{+0.06}_{-0.07}$	$1.01^{+0.08}_{-0.09}$	$0.91^{+0.28}_{-0.27}$	$10.49^{+0.10}_{-0.10}$	34.7/43
93433-01-02-01	54561.0	$1.70^{+0.05}_{-0.05}$	$1.14^{+0.08}_{-0.09}$	$0.80^{+0.27}_{-0.27}$	$11.41^{+0.08}_{-0.08}$	28.7/43
93433-01-02-02	54561.7	$1.72^{+0.07}_{-0.07}$	$1.06^{+0.09}_{-0.11}$	$0.70^{+0.28}_{-0.27}$	$9.43^{+0.09}_{-0.09}$	27.1/43
93433-01-02-03	54562.7	$1.76^{+0.05}_{-0.05}$	$1.00^{+0.12}_{-0.12}$	$0.44^{+0.23}_{-0.21}$	$10.13^{+0.07}_{-0.07}$	40.6/43
93433-01-02-04	54563.8	$1.73^{+0.07}_{-0.07}$	$1.11^{+0.12}_{-0.12}$	$0.70^{+0.30}_{-0.30}$	$10.11^{+0.09}_{-0.09}$	34.9/43
93433-01-02-05	54566.2	$1.73^{+0.10}_{-0.12}$	$1.31^{+0.34}_{-0.22}$	$0.86^{+0.67}_{-0.65}$	$12.51^{+0.19}_{-0.19}$	45.3/43
93433-01-02-06	54566.3	$1.70^{+0.06}_{-0.06}$	$1.03^{+0.10}_{-0.12}$	$0.74^{+0.30}_{-0.29}$	$11.13^{+0.10}_{-0.10}$	30.8/43
93433-01-02-07	54566.8	$1.76^{+0.07}_{-0.07}$	$1.05^{+0.09}_{-0.11}$	$0.69^{+0.27}_{-0.27}$	$8.60^{+0.08}_{-0.08}$	41.8/43
93433-01-03-00	54568.6	$1.69^{+0.05}_{-0.05}$	$1.13^{+0.06}_{-0.06}$	$0.95^{+0.23}_{-0.23}$	$11.26^{+0.07}_{-0.07}$	25.2/43
93433-01-03-01	54570.3	$1.80^{+0.05}_{-0.06}$	$1.02^{+0.11}_{-0.14}$	$0.47^{+0.24}_{-0.22}$	$9.27^{+0.07}_{-0.07}$	35.5/43
93433-01-03-02	54572.3	$1.74^{+0.04}_{-0.04}$	$1.04^{+0.08}_{-0.09}$	$0.58^{+0.19}_{-0.19}$	$10.37^{+0.06}_{-0.06}$	38.1/43
93433-01-04-00	54574.3	$1.72^{+0.06}_{-0.06}$	$1.06^{+0.09}_{-0.11}$	$0.68^{+0.27}_{-0.26}$	$10.24^{+0.08}_{-0.08}$	27.8/43
93433-01-04-01	54576.3	$1.79^{+0.06}_{-0.06}$	$1.02^{+0.12}_{-0.17}$	$0.49^{+0.27}_{-0.26}$	$9.82^{+0.08}_{-0.08}$	35.4/43
93433-01-04-02	54578.7	$1.70^{+0.05}_{-0.05}$	$1.01^{+0.06}_{-0.07}$	$0.82^{+0.19}_{-0.18}$	$9.54^{+0.06}_{-0.06}$	20.6/43
93433-01-04-03	54579.8	$1.75^{+0.06}_{-0.06}$	$0.96^{+0.07}_{-0.09}$	$0.75^{+0.22}_{-0.21}$	$8.61^{+0.08}_{-0.08}$	30.8/43
93433-01-04-04	54580.6	$1.80^{+0.05}_{-0.05}$	$0.94^{+0.11}_{-0.14}$	$0.42^{+0.20}_{-0.18}$	$8.90^{+0.07}_{-0.07}$	37.8/43
93433-01-05-00	54581.4	$1.80^{+0.08}_{-0.08}$	$0.97^{+0.12}_{-0.15}$	$0.48^{+0.26}_{-0.24}$	$7.80^{+0.09}_{-0.09}$	34.8/43
93433-01-05-01	54582.7	$1.78^{+0.06}_{-0.06}$	$0.93^{+0.10}_{-0.12}$	$0.54^{+0.21}_{-0.20}$	$8.22^{+0.08}_{-0.08}$	40.1/43
93433-01-05-02	54583.5	$1.71^{+0.06}_{-0.06}$	$1.00^{+0.08}_{-0.10}$	$0.65^{+0.21}_{-0.20}$	$9.11^{+0.07}_{-0.07}$	27.0/43
93433-01-05-03	54584.7	$1.80^{+0.05}_{-0.06}$	$0.97^{+0.10}_{-0.12}$	$0.42^{+0.17}_{-0.16}$	$7.28^{+0.06}_{-0.06}$	45.0/43
93433-01-05-04	54585.6	$1.78^{+0.07}_{-0.07}$	$0.83^{+0.10}_{-0.13}$	$0.44^{+0.16}_{-0.15}$	$6.26^{+0.06}_{-0.06}$	62.3/43
93433-01-05-05	54586.7	$1.79^{+0.07}_{-0.07}$	$0.95^{+0.11}_{-0.14}$	$0.46^{+0.21}_{-0.20}$	$6.98^{+0.07}_{-0.07}$	37.7/43
93433-01-05-06	54587.8	$1.79^{+0.05}_{-0.05}$	$0.84^{+0.08}_{-0.09}$	$0.43^{+0.12}_{-0.11}$	$6.34^{+0.05}_{-0.05}$	24.3/43
93433-01-06-00	54588.1	$1.77^{+0.08}_{-0.08}$	$0.77^{+0.12}_{-0.13}$	$0.44^{+0.18}_{-0.16}$	$6.32^{+0.08}_{-0.08}$	32.5/43
93433-01-06-01	54588.1	$1.82^{+0.07}_{-0.07}$	$0.80^{+0.14}_{-0.18}$	$0.32^{+0.18}_{-0.15}$	$6.47^{+0.07}_{-0.07}$	40.0/43
93433-01-06-02	54590.7	$1.82^{+0.07}_{-0.07}$	$0.85^{+0.11}_{-0.13}$	$0.42^{+0.18}_{-0.16}$	$6.63^{+0.07}_{-0.07}$	20.1/43
93433-01-06-03	54591.7	$1.71^{+0.05}_{-0.06}$	$0.98^{+0.06}_{-0.07}$	$0.64^{+0.15}_{-0.15}$	$6.92^{+0.05}_{-0.05}$	37.1/43
93433-01-06-04	54592.8	$1.73^{+0.09}_{-0.09}$	$0.98^{+0.08}_{-0.09}$	$0.67^{+0.22}_{-0.21}$	$6.18^{+0.08}_{-0.08}$	20.2/43
93433-01-06-05	54593.7	$1.79^{+0.06}_{-0.06}$	$0.87^{+0.08}_{-0.09}$	$0.47^{+0.15}_{-0.14}$	$6.03^{+0.06}_{-0.06}$	33.2/43
93433-01-07-00	54598.2	$1.80^{+0.14}_{-0.16}$	$0.77^{+0.14}_{-0.16}$	$0.39^{+0.21}_{-0.19}$	$4.08^{+0.10}_{-0.10}$	35.1/43
93433-01-07-02	54601.3	$1.80^{+0.08}_{-0.08}$	$0.72^{+0.17}_{-0.17}$	$0.30^{+0.16}_{-0.14}$	$5.75^{+0.08}_{-0.08}$	23.3/43
93433-01-08-00	54602.6	$1.92^{+0.10}_{-0.11}$	$0.71^{+0.17}_{-0.24}$	$0.25^{+0.17}_{-0.15}$	$4.63^{+0.08}_{-0.08}$	22.7/43
93433-01-08-01	54604.7	$1.99^{+0.06}_{-0.06}$	$0.65^{+0.13}_{-0.16}$	$0.16^{+0.10}_{-0.08}$	$4.28^{+0.05}_{-0.05}$	38.0/43
93433-01-08-02	54606.7	$1.92^{+0.06}_{-0.06}$	$0.72^{+0.11}_{-0.14}$	$0.23^{+0.10}_{-0.09}$	$4.93^{+0.05}_{-0.05}$	38.5/43
93433-01-08-03	54608.7	$2.05^{+0.03}_{-0.03}$	$0.05^{+0.25}_{-0.04}$	$0.01^{+0.01}_{-0.01}$	$4.21^{+0.05}_{-0.05}$	44.7/43
93433-01-08-04	54606.0	$1.98^{+0.07}_{-0.09}$	$0.49^{+0.25}_{-0.36}$	$0.14^{+0.14}_{-0.08}$	$4.78^{+0.07}_{-0.07}$	32.1/43
93433-01-09-00	54609.4	$1.96^{+0.09}_{-0.10}$	$0.61^{+0.16}_{-0.25}$	$0.20^{+0.13}_{-0.11}$	$3.99^{+0.07}_{-0.07}$	23.2/43
93433-01-09-01	54610.4	$1.92^{+0.09}_{-0.10}$	$0.79^{+0.11}_{-0.14}$	$0.29^{+0.13}_{-0.13}$	$3.86^{+0.05}_{-0.05}$	26.9/43
93433-01-09-02	54611.5	$1.94^{+0.06}_{-0.06}$	$0.63^{+0.11}_{-0.13}$	$0.22^{+0.09}_{-0.08}$	$4.44^{+0.05}_{-0.05}$	26.2/43
93433-01-09-03	54612.4	$2.10^{+0.09}_{-0.15}$	$0.55^{+0.32}_{-0.54}$	$0.10^{+0.08}_{-0.08}$	$3.43^{+0.08}_{-0.08}$	31.9/43
93433-01-09-04	54613.6	$1.98^{+0.09}_{-0.10}$	$0.61^{+0.16}_{-0.24}$	$0.19^{+0.13}_{-0.11}$	$3.81^{+0.07}_{-0.07}$	34.0/43
93433-01-10-00	54618.8	$2.00^{+0.09}_{-0.10}$	$0.53^{+0.16}_{-0.22}$	$0.15^{+0.09}_{-0.07}$	$3.10^{+0.05}_{-0.05}$	26.4/43
93433-01-10-02	54622.0	$1.97^{+0.14}_{-0.15}$	$0.65^{+0.16}_{-0.29}$	$0.21^{+0.15}_{-0.13}$	$3.02^{+0.07}_{-0.07}$	26.0/43
93433-01-11-00	54624.8	$2.01^{+0.11}_{-0.12}$	$0.67^{+0.14}_{-0.23}$	$0.17^{+0.11}_{-0.10}$	$2.76^{+0.05}_{-0.05}$	35.2/43
93433-01-11-01	54628.1	$2.01^{+0.20}_{-0.21}$	$0.72^{+0.21}_{-0.71}$	$0.18^{+0.11}_{-0.13}$	$2.52^{+0.08}_{-0.08}$	24.5/43
93433-01-12-00	54631.8	$1.98^{+0.14}_{-0.15}$	$0.67^{+0.12}_{-0.18}$	$0.18^{+0.10}_{-0.09}$	$2.08^{+0.05}_{-0.05}$	29.9/43
93433-01-12-01	54636.7	$1.99^{+0.19}_{-0.17}$	$0.70^{+0.16}_{-0.56}$	$0.17^{+0.07}_{-0.08}$	$2.32^{+0.06}_{-0.06}$	34.3/43

Table 3. An additional BB component is included in the spectral fitting. f_{BB} : unabsorbed (3–25 keV) flux of BB component in units of 10^{-10} erg cm $^{-2}$ s $^{-1}$. Flux: 3–25 keV unabsorbed flux in units of 10^{-10} erg cm $^{-2}$ s $^{-1}$. All errors are at the 90% confidence level.

ACKNOWLEDGEMENTS

We thank the referee for helpful comments which significantly improved this work. We are grateful to Long Ji for help discussions on type I X-ray burst data analysis. This work is partially supported with funding by 973 Program of China under grant 2014CB845802, the National Natural Science Foundation of China under grants 11133002, 11373036, and 11303022, the Qianren start-up grant 292012312D1117210, and by the Strategic Priority Research Program “The Emergence of Cosmological Structures” of the Chinese Academy of Sciences, Grant No. XDB09000000. S.S.W. is funded by the Co-Circulation Scheme, supported by the EC-FP7 Marie Curie Actions-People-COFUND and TÜBİTAK.

REFERENCES

- Allen, J. L., Linares, M., Homan, J., & Chakrabarty, D. 2015, *ApJ*, 801, 10
- Armas Padilla, M., Degenaar, N., Patruno, A., Russell, D. M., Linares, M., Maccarone, T. J., Homan, J., Wijnands, R., 2011, *MNRAS*, 417, 659
- Basinska, E. M., Lewin, W. H. G., Sztajno, M., Cominsky, L. R., & Marshall, F. J. 1984, *ApJ*, 281, 337
- Belloni T. M., 2010, in Belloni T., ed., *The Jet Paradigm C From Microquasars to Quasars*. *Lect. Not. Phys.*, 794, 53. Springer Verlag, Berlin
- Done, C., Gierliński M., & Kubota, A. 2007, *A&ARv*, 15, 1D
- Dunn R. J. H., Fender R. P., Körding E. G., Belloni T., Cabanac C., 2010, *MNRAS*, 403, 61
- Galloway, D. K., Muno, M. P., Hartman, J. M., Psaltis, D., Chakrabarty, D., 2008, *ApJS*, 179, 360
- Gierliński, M. & Done, C. 2002, *MNRAS*, 337, 1373
- Hasinger, G., & van der Klis, M. 1989, *A&A*, 225, 79
- Heil L. M., Vaughan S., Uttley P., 2012, *MNRAS*, 422, 2620
- Kuulkers, E., den Hartog, P. R., in’t Zand, J. J. M., Verbunt, F. W. M., Harris, W. E., Cocchi, M., 2003, *A&A*, 399, 663
- Lewin, W. H. G., van Paradijs, J., & Taam, R. E. 1993, *Space Sci. Rev.*, 62, 223
- Lattimer, J. M., & Prakash, M. 2007, *Phys. Rep.*, 442, 109
- Lin, D., Remillard, R. A., & Homan, J. 2007, *ApJ*, 667, 1073
- Liu, Q. Z., van Paradijs, J., & van den Heuvel, E. P. J. 2006, *A&A*, 455, 1165
- Liu, Q. Z., van Paradijs, J., & van den Heuvel, E. P. J. 2007, *A&A*, 469, 807
- Markwardt, C. B., Strohmayer, T. E., & Swank, J. H. 2008, *Astron. Telegram*, 1443, 1
- Migliari, S., & Fender, R. P., 2006, *MNRAS*, 366, 79
- Miyamoto S., Kimura K., & Kitamoto S., 1991, *ApJ*, 383, 784
- Muno, M. P., Remillard, R. A., & Chakrabarty, D. 2002, *ApJL*, 568, L35
- Muñoz-Darias, T., Coriat, M., Plant, D. S., Ponti, G., Fender, R. P., Dunn, R. J. H., 2013, *MNRAS*, 432, 1330
- Muñoz-Darias, T., Fender, R. P., Motta, S. E., Belloni, T. M. 2014, *MNRAS*, 443, 3270
- Muñoz-Darias, T., Motta, S. E., Belloni, T. M. 2011, *MNRAS*, 410, 679
- Narayan, R., & McClintock, J.E. 2008, *New Astron. Rev.*, 51, 733
- Plotkin, R. M., Gallo, E., & Jonker, P. G. 2013, *ApJ*, 773, 59
- Starling, R., Kennea, J., & Krimm, H. 2008, *Astron. Telegram*, 1441, 1
- Steiner, A. W., Lattimer, J. M., & Brown, E. F. 2010, *ApJ*, 722, 33
- Weng, S. S., & Zhang, S. N. 2011, *ApJ*, 739, 42
- Wijnands, R., Degenaar, N., Armas Padilla M., Altamirano, D., Cavecchi, Y., Linares, M., Bahramian, A., Heinke, C. O., 2014, *arXiv:1409.6265*
- van der Klis, M. 2006, in *Compact Stellar X-ray Sources*, ed. W. Lewin & M. van der Klis (Cambridge: Cambridge Univ. Press), 39